Theor Chim Acta (1988) 74: 445-461

Theoretica Chimica Acta

All-valence-electron and transition density matrix calculations of the electronic spectra of [2.2]paracyclophanequinones

Antoni K. Wisor and Leszek Czuchajowski

Department of Chemistry, University of Idaho, Moscow, ID 83843, USA

(Received October 6, 1987, revised January 14/Accepted April 4, 1988)

The combined CNDO/S and transition density matrix methods reproduced well the UV-VIS spectra of the intramolecular charge-transfer complexes of double- and triple-layered [2.2]paracyclophanequinones in which benzene and *p*-benzoquinone represent the donor and acceptor layers: ***DA***, ***DDA*** and ***DAD***. Calculations pointed to the already known experimental bathochromic shifts of the longest wavelength absorption band for the ***DA*** → ***DDA*** → ***DAD*** transformations. The electronic transitions corresponding to this band are for ***DA*** and ***DDA*** the CT transitions of the $\pi \rightarrow \pi^*$ type; however, for ***DAD*** the band represents the $n \rightarrow \pi^*$ transition localized on the acceptor ring.

Key words: CNDO/S method for intramolecular CT complexes — Transition density matrix method — Electronic spectra of the [2.2]paracyclophanequinones

1. Introduction

The intramolecular charge-transfer (CT) complexes in which both the π-donor, ***D***, and π-acceptor, ***A***, constitute the layers of the rigid cyclophane skeleton were already the subject of investigations of transannular interactions [1-7]. Of particular interest in this group of compounds are the structures in which benzene (B) [1, 3] or hydroquinone (H) [2] is ***D***, and *p*-benzoquinone (Q) is ***A***. Our interest is focused in this paper on the double-layered [2.2]paracyclophanequinone (PCPQ) ***DA***, **1**, and the corresponding triple-layered [2.2]paracyclophanequinones ***DDA***, **2** and ***DAD***, **3**, see Fig. 1, representing different sequence of stacked benzene ***D*** and *p*-benzoquinone ***A***, rings. These compounds

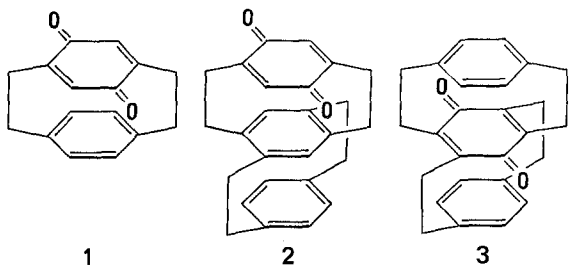

Fig. 1. The paracyclophanequinones under consideration: **1**, the double-layered [2.2]paracyclophanequinone; **2** and **3**, the isomeric triple-layered [2.2]paracyclophanequinones. These three structures represent, respectively, the ***DA***, ***DDA*** and ***DAD*** intramolecular complexes. Models **I**, **II** and **III** appearing in the text and Figs. 2, 3, and 4 correspond to the above structures but do not contain bridges between the rings

have never been treated theoretically; only Vogler [5-7], in order to explain the transannular interactions, performed quantum chemical calculations in the π-electron approximation on "intramolecular quinhydrones", using the UV-VIS spectra as an experimental reference.

In the electronic spectra of the PCPQ structures **1**, **2** and **3** a characteristic broad absorption band can be observed in the long wavelength region, see Fig. 2. It results, seemingly, from the intramolecular electron transfer; λ_{max} (ε): **1**, 340 nm (597) [1]; **2**, 395 nm (2330); **3**, 435 nm (320) [3]. It is interesting, however, to learn whether the charge transfer is the only reason for such a substantial

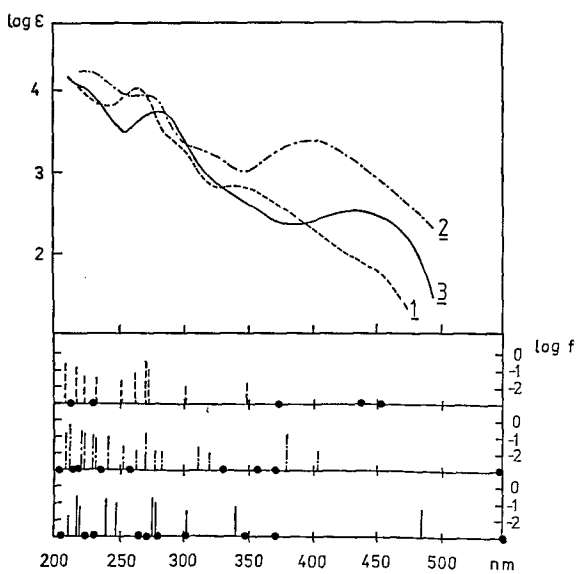

Fig. 2. *Top*: The experimental UV-VIS spectra of [2.2]paracyclophanequinones **1**, **2** and **3** according to Cram and Day [1] and Misumi et al. [3]. *Bottom*: Spectra calculated by CNDO/S-CIS. *Dots* show the positions of transitions characterised by $f < 0.001$

bathochromic shift in this series of structures. In solving this problem it is crucial to choose a proper calculational method. This system cannot be limited to the π-electron approximation; therefore, we applied the all-valence-electron (AVE) approach. To the description of the electronic transitions we used the transition density matrix (TDM) method [8] which was previously used by us in the investigation of the electronic structure of cyclophanes and heterophanes [9–11].

It is of additional interest that the class of intramolecular CT complexes investigated in this paper might represent compounds, the properties of which would allow them to serve as molecular information carriers based on modification of the electronic structure [12].

2. Theoretical treatment

Our theoretical approach was based on: (1) MO theory in the supermolecule approximation; (2) consideration of the σ–π interaction and σ–π polarization; (3) calculation of the transition energies and oscillator strengths by CNDO/S method with the interaction of single excited configurations, CIS (4) transition density matrix method in AVE approximation applied to the analysis of the excited states.

Until now, the supermolecule approximation was applied to the layered compounds mainly in the framework of π-electron methods [5–7, 10, 11, 13, 14]. The reason for this was the large size of the molecules considered. However, these methods do not allow one to consider in a direct way the σ–π interaction [14] between the σ orbitals of the ethane bridges and the π orbitals of aromatic rings, and also the σ–π polarization between the same orbitals in rings. Our previous treatment [9] was exceptional that we went beyond the π-electron approximation and successfully applied the CNDO/S method of Del Bene and Jaffe [16] to some cyclophanes and heterophanes. In the present paper we extend the use of the CNDO/S method to the PCPQ structures in spite of some opinions of its inapplicability to the explanation of some spectral properties of phanes. To the latter belong those which originate either from the transannular interactions [17] or from the intramolecular charge transfer [6]. The former case has been demonstrated incorrect by our previous calculations [9], the latter by the results presented here. The difficulty in explaining the influence of the intramolecular CT on the electronic spectra of PCPQs arose from incorrect parametrization for the oxygen atom used in the original CNDO/S method. The change in parametrization proposed by one of the authors [18] was based on research concerning quinone [19] to which also Jaffe et al. [20] referred. The change consisted only of acceptance for the one-centered resonance integral the value of -27 eV instead -45 eV used in the original parametrization. Beside this change it appeared also necessary to consider the long expansion in the CIS method, namely 100 configurations for **1** and 130 for **2** and **3**. In the calculations, the diagonalization procedure by the Householder-QR-inverse-iteration [21a] method was applied; the latter was modified by one of the authors [21b].

The investigation of the electronic transitions can be performed with the use of orbital-configurational analysis. Applying the CNDO/S method, the self-consistent MO (occupied $|i\rangle$ and virtual$|p\rangle$) of the ground state $|\Phi\rangle$ can be found, representing the linear combination of atomic orbitals $|\mu\rangle$ (LCAO). Then, the CIS method gives the following approximation of the excited state

$$|\Phi^*\rangle = \sum_{i=1}^{n} \sum_{p=n+1}^{m} d_{pi} |\Phi_i \to p\rangle, \tag{1}$$

where d_{pi} are the CI coefficients and the determinantal functions $|\Phi_i \to p\rangle$ are obtained from $|\Phi\rangle$ as a result of the exchange of MO$|i\rangle$ to $|p\rangle$. However, searching for the LCAO and CI coefficients of the greatest values in the great number of data is very tedious for such large structures as the PCPQs under consideration. On the other hand such a presentation of the set of numbers would be poorly readable.

In order to calculate the electronic states of the molecule according to the approximation, Eq. (1), one can take advantage of the quantum chemistry approach based on the formalism of the transition density matrix [8a]. In this case the basic equation can be presented as the eigenvalue problem of certain superoperator, for which each eigenvector plays a role of the transition density matrix D of any chosen excited state and the eigenvalue of this superoperator gives the energy of excitation λ [8b]. The transition matrix D takes then the form

$$D = \sum_{i=1}^{n} \sum_{p=n+1}^{m} (d_{pi} |p\rangle\langle i| + d_{pi}^* |i\rangle\langle p|), \tag{2}$$

where d_{pi} can be treated as the CI coefficients of the excited state described by Eq. (1). With the use of the superoperator, one can calculate the matrix D simultaneously with the energies of excitations λ. Because of the form of the transition density matrix D presented in Eq. 2, we calculated that matrix in two steps, first finding the form of MO$|i\rangle$ and $|p\rangle$ by the CNDO/S method and then finding the d_{pi} coefficients by the CIS method.

The case of PCPQ proves particularly well the universal character of the TDM method [8] as a simple theoretical tool enabling the correct and possibly complete interpretation of spectral properties of molecules. Besides being useful in the assignment of the type of electronic transition (e.g. $n \to \pi^*$, $\sigma \to \pi^*$, $\pi \to \pi^*$ etc.) [9] or the size of transannular interaction [10], this method can also be helpful in estimating the size of the charge transferred in the CT states. The localization number L_A [22], which is the basic magnitude of the TDM method, describes the participation of the molecular fragment A in the excitation

$$L_A = \sum_{\mu \in A} \langle \mu | D^2 | \mu \rangle, \tag{3}$$

where D represents the TDM. When each atom provides to the valence shell the atomic orbitals $|\mu\rangle$ of different type (e.g. n, σ, π, π^* etc.), then all valence orbitals of the atoms belonging to the fragment A are included in the summation. If the molecule can be divided into several fragments, A+B+ $\cdots$ +Z, the sum of localization numbers (Eq. (3)) corresponding to these fragments equals, ex

definitio, 100%. Total localization of the excitation on the specific molecular fragment, e.g. A, consists of the local excitation on the fragment (partial localization number 1_A), the transfer of charge from this fragment to all remaining fragments (charge-transfer localization numbers $l_{A\to B}, \ldots, l_{A\to Z}$), and the reverse transfers ($l_{B\to A}, \ldots, l_{Z\to A}$, respectively)

$$L_A = l_A + 1/2^*(l_{A\to B} + l_{B\to A} + \cdots + l_{A\to Z} + l_{Z\to A}). \tag{4}$$

In this approach a very characteristic dependency exists between the transfer of charge which accompanies the appearance of the CT states characterized by the $l_{A\to B}$, $l_{B\to A}$ etc. numbers, and the observed charge transfer. The latter corresponds to change of electron density Δq_A on the molecular fragment A during the excitation

$$\Delta q_A = \sum_{B\neq A} (l_{B\to A} - l_{A\to B}). \tag{5}$$

The increase of the electron density on the fragment A takes place exclusively at the expense of the states of charge transfer from the remaining molecular fragments to the fragment A. The states corresponding to the electron transfer from A to the remaining molecular fragments only diminish Δq_A. Because the latter represents a difference of two values, only in the presence of a very strong donor or acceptor would one of the components disappear from Eq. (5) (that is $l_{B\to A}$ for ***D***, and $l_{A\to B}$ for ***A***). Then Δq_A becomes equivalent to the weight of the CT states, i.e. to $l_{A\to B}$ or $l_{B\to A}$.

The choice of the localization number L_A given by Eq. (3) as a measure of localization is based on a different type of considerations. Namely, Luzanov et al. [22a] applied to the description of localization of excitation the modulus of the operator of the change of density matrix at the excitation, $|\Delta\rho|$, which is equivalent to the D^2 matrix if the assumed form of excited state wave function is the same as in the CIS method, Eq. (1). Therefore, the L_A numbers automatically express the changes of both charges and bond orders at the excitation. Because of that, the traditional and commonly used approach to the evaluation of the localization of transition which is based on one of these magnitudes only (e.g. changes of charges) does not seem to be justified [22*d*]. This is the reason why we give a preference to the localization numbers originating from investigation of the TDM over other indices [23].

The crystal structures of the PCPQ **1**, **2** and **3** compounds are not available; therefore, an indirect approach was applied in which the crystallographic data of [2.2]paracyclophane (PCP) [24] were used for the B ring and those of [2.2]-(2,5)benzoquinophane (BQP) [25] - for the Q ring. In the latter compound the Q rings are boat-shaped (like the B rings in PCP) but they retain the bond lengths typical of *p*-benzoquinone [26]. In the calculations concerning the structure **1** those mean distances were applied which were found in PCP and BQP between the atoms located in the opposing rings. As a result of this, the mean inter-ring distance for **1** equals 3.2 Å. In compounds **2** and **3**, the inner ring was considered as twist-shaped and the geometry was assumed also with the use of X-ray data of the multilayered cyclophanes [27].

3. Results

The results of calculations are present in Table 1 and Fig. 2. The C_2 point group was considered for the symmetry of excited states. The type of transition was defined in accordance with the analysis of TDM.

The calculations show for all PCPQs considered that the longest wavelength transition represents the $\pi \rightarrow \pi^*$ low-intensity transition to the 1^1A excited state. The corresponding wavelength is smaller for **1** than for **2** and **3**. The values for the latter two compounds are similar. This agrees with the fact, reflected also by the UV-VIS spectra, that the long wavelength absorption begins at the same wavelengths for **2** and **3** and is bathochromatically shifted with regard to **1**, see Fig. 2. The character of the transition is ambiguous. Depending on the type of PCPQ, it represents a different extent of transfer of the charge, Δq_Q to the Q ring (+0.55e for **1**, +0.81e for **2** and +0.30e for **3**). The transition is pure CT only in the case of **2**; for the remaining compounds it has a mixed character because of the participation of the local excitation of the Q ring, which for **3** amounts to 60%. This transition has, however, a very low intensity (especially for **2**) and because of that it can not be connected with the observed long wavelength absorption band in any of the PCPQs.

The second long wavelength transition is the $n \rightarrow \pi^*$ transition to the 1^1B excited state. It has a low, although different intensity, which increases in the order of $\mathbf{1} < \mathbf{2} < \mathbf{3}$. The wavelength at which the transition takes place decreases in the order of $\mathbf{3} > \mathbf{1} > \mathbf{2}$. This allows one to assign the regarded transition in **3** (486.4 nm, $f = 0.049$) to the broad long wavelength band having the maximum at 435 nm, $\varepsilon = 320$. This assignment is even more justified because the next transitions are quite distant as far as its energy value is concerned. All $n \rightarrow \pi^*$ transitions are totally localized on the Q ring and take place in the framework of the carbonyl groups, i.e. very much in the same way as in *p*-benzoquinone and its methyl derivatives [18].

With regard to the transitions of the CT character, marked by their relatively high intensity, it can be said that they represent transitions to the 3^1A, 2^1A and 4^1A excited states, for **1**, **2** and **3**, respectively. The $^1A \rightarrow 2^1A$ transition for **2** is distinguished by the high intensity ($f = 0.159$, while only 0.016 for **1** and 0.060 for **3**) which in connection with calculated wavelength of 380.0 nm agrees well with the observed values, 395 nm ($\varepsilon = 2330$). In this case the size of the charge transfer into the Q ring is the greatest, $\Delta q_Q = +0.91$e; the contribution of the transfer from the inner B rings is −0.67e, from the outer B ring −0.24e. Also in the case of **1**, the $^1A \rightarrow 3^1A$ transition at 348.2 nm is assigned to the maximum observed at 340 nm ($\varepsilon = 597$) belonging to the long wavelength absorption band. The charge transferred is smaller now, $\Delta q_Q = +0.58$e. The CT transition to the 4^1A state for **3**, situated higher in energy than the $n \rightarrow \pi^*$ transition, corresponds almost to the same wavelength 338.6 nm as the analogous transition in **1**. The additional charge appearing as a result of this transition on the Q ring, $\Delta q_Q = +0.76$e, is uniformly transferred from both B rings. Such a location of the CT transition in **3** is suggested by the observed increase of absorption in the region

Table 1. Calculated electronic transitions in double- and triple-layered [2.2]paracyclophanequinones

Double-layered [2.2]paracyclophanequinone, **1** (***DA*** complex)				Triple-layered [2.2]paracyclophanequinone, **2** (***DDA*** complex)				Triple-layered [2.2]paracyclophanequinone, **3** (***DAD*** complex)			
Symm.	Type	λ, nm	*f*	Symm.	Type	λ, nm	*f*	Symm.	Type	λ, nm	*f*
1^1A	$\pi \rightarrow \pi^*$(CT, Q)	451.7	0.009	1^1A	$\pi \rightarrow \pi^*$(CT)	545.9	0.001	1^1A	$\pi \rightarrow \pi^*$(Q, CT)	552.2	0.021
1^1B	$n \rightarrow \pi^*$ (Q)	435.8	0.004	1^1B	$n \rightarrow \pi^*$(Q)	404.3	0.019	1^1B	$n \rightarrow \pi^*$(Q)	486.4	0.049[c]
2^1A	$n \rightarrow \pi^*$ (Q)	372.3	0.000	2^1A	$\pi \rightarrow \pi^*$(CT)	380.0	0.159[b]	2^1A	$\pi \rightarrow \pi^*$ (CT)	372.2	0.000
3^1A	$\pi \rightarrow \pi^*$ (CT)	348.2	0.016[a]	3^1A	$n \rightarrow \pi^*$(Q)	371.4	0.001	3^1A	$n \rightarrow \pi^*$(Q)	347.4	0.000
2^1B	$\pi \rightarrow \pi^*$(B)	301.2	0.013	2^1B	$\pi \rightarrow \pi^*$(B)	356.8	0.002	4^1A	$\pi \rightarrow \pi^*$ (CT)	338.6	0.060
4^1A	$\pi \rightarrow \pi^*$ (CT)	273.0	0.127	4^1A	$\pi \rightarrow \pi^*$ (Q)	329.1	0.004	2^1B	$\pi \rightarrow \pi^*$ (B)	303.8	0.015
3^1B	$\pi \rightarrow \pi^*$(Q)	271.7	0.387	3^1B	$\pi \rightarrow \pi^*$ (B)	319.0	0.013	3^1B	$\pi \rightarrow \pi^*$ (Q, B)	302.2	0.051
				4^1B	$\pi \rightarrow \pi^*$ (B)	308.9	0.023	4^1B	$\pi \rightarrow \pi^*$ (Q, B)	300.1	0.005
				5^1A	$\pi \rightarrow \pi^*$ (CT)	285.1	0.013	5^1B	$\pi \rightarrow \pi^*$ (CT)	279.5	0.000
				5^1B	$\pi \rightarrow \pi^*$ (mix.)	279.6	0.017	6^1B	$\pi \rightarrow \pi^*$ (Q)	278.7	0.129
				6^1B	$\pi \rightarrow \pi^*$(Q)	271.5	0.193	5^1A	$\pi \rightarrow \pi^*$ (CT)	276.7	0.199

[a] Exp. value 340 nm ($\varepsilon = 579$) [1]
[b] Exp. value 395 nm ($\varepsilon = 2330$) [3]
[c] Exp. value 435 nm ($\varepsilon = 320$) [3]

ca. 350 nm. This is another indication that the long wavelength absorption appearing in **3** cannot be related to the CT transition.

The calculations also reproduce well other spectroscopic features common for all considered PCPQs, like the greatest intensity of absorption appearing in the 250–300 nm region. The calculations show that this absorption corresponds to the $\pi \rightarrow \pi^*$ transition, excited locally only on the Q ring which originates from the short wavelength, intense, $\pi \rightarrow \pi^*$ transition in *p*-benzoquinone [17].

Also the $\pi \rightarrow \pi^*$ transitions appear localized on the B rings. Their low intensity remain in accordance with the assignment. They are shifted bathochromically with regard to the corresponding α band in benzene what suggests the appearance of transannular interactions in PCPQs. This fact is reflected by a small shoulder on the absorption curves in the region of ca. 300 nm.

4. Discussion

As one can see, the $\pi \rightarrow \pi^*$ transitions of CT character can be ascribed to the long wavelength band in the UV-VIS spectra of **1** and **2**. In contrast, in **3** for the long wavelength band accounts the $n \rightarrow \pi^*$ transition. The CT transition appears quite behind the $n \rightarrow \pi^*$ transition. The correctness of these assignments is demonstrated by the low intensity of the long wavelength absorption band in **3**. Nevertheless, we gave particular attention to the behaviour of the CT transitions in the investigated PCPQs by applying three model structures **I**, **II** and **III**, which correspond to the real PCPQs **1**, **2** and **3**, respectively. In model **I** representing two stacked planar Q and B rings, the rings were approached along the mutual C_2 axis (z) from a distance of 4 to 3 Å. Model **II** consists of model **I** (in which the inter-ring distance of 3.2 Å was kept constant) to which from the side of the B ring another B ring was approached at a distance ranging from 4 to 3 Å. In model **III** the second B ring was approached from the side of the Q ring. All these models represent the same symmetry (C_{2v}) in the range of distances considered. The results of calculations are shown in Figs. 3–5 and Table 2.

Careful consideration of the ground state of model **I** would allow a better understanding of the excited states in all three models. Focussing attention on model **I** only, is reasonable because of the way in which the two remaining models were formed from it. In Fig. 3 (left) the changes of the MOs energy are shown in dependence on the inter-ring Q-B distance. The analysis of the LCAO coefficients shows that the n orbitals are totally localized on the Q ring, independently of the distance. The π and π^* orbitals show different localization on the particular rings, as described by the characteristics of the seven frontier MOs, Fig. 3 (center). For the starting inter-ring distance of 4 Å the localization is unambiguously defined, and a given set of energy levels results from the overlapping of energy levels in the isolated molecules of *p*-benzoquinone [18, 20] and benzene [16, 18]. For example, the HOMO of $9b_1$ symmetry and $9b_2$ orbital have similar orbital energies and are totally localized on the B ring. The LUMO of $10b_2$ symmetry is totally localized on the Q ring. During the mutual approach of Q and B rings, the sequence of the energy levels does not change, while the

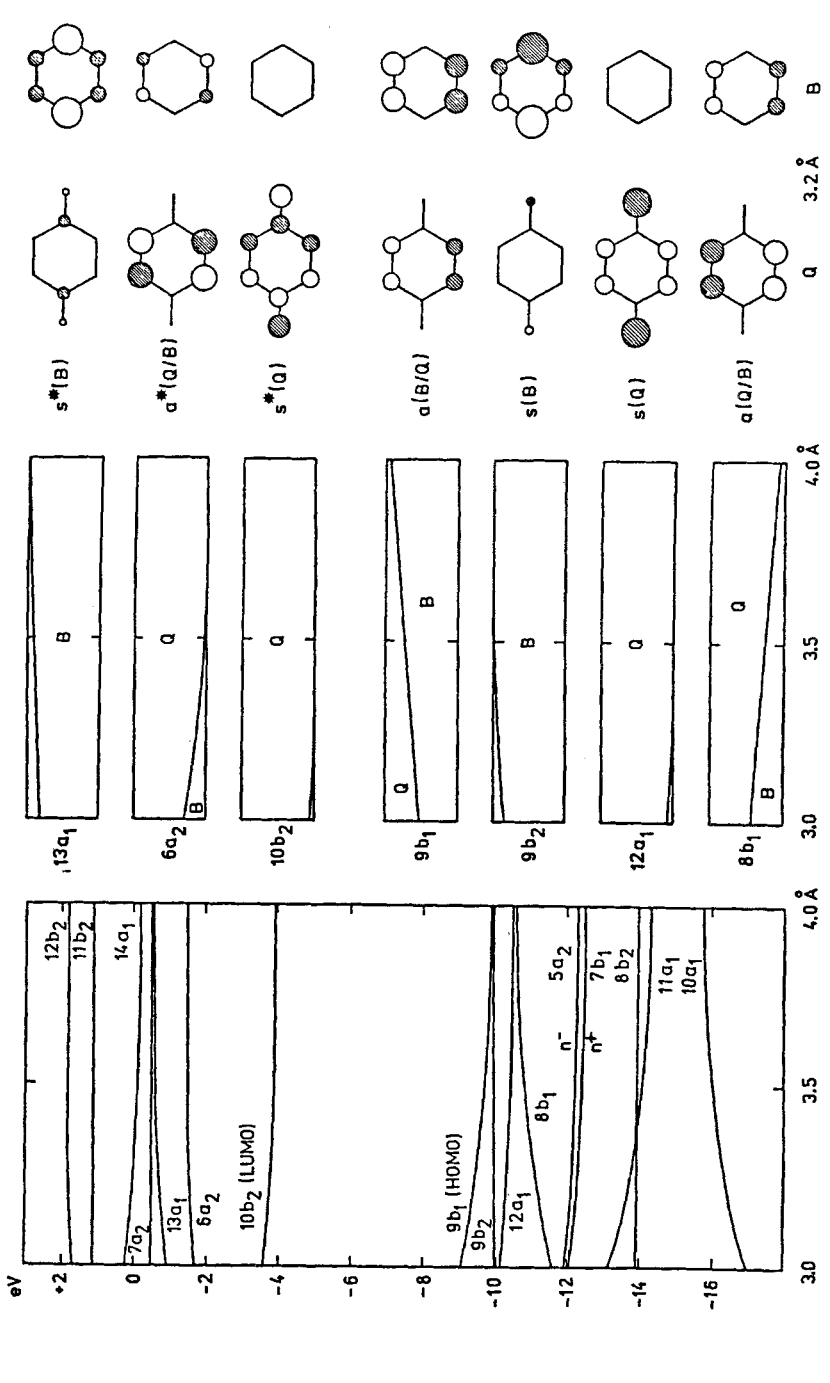

Fig. 3. The characteristics of the ground state in model 1. *Left*: the changes of the MOs energy (eV) vs the inter-ring Q–B distance (Å). Except for two *n*-type orbitals all MOs represent the π or π^* orbitals. *Center*: the localization on the Q and B rings of the seven frontier π-MOs vs the inter-ring Q–B distance. The degree of localization on a particular ring is expressed by the sum of the squares of the LCAO coefficients related to the ring. *Right*: spatial features of the seven frontier π-MOs for the inter-ring Q–B distance 3.2 Å, given in terms of the contribution of positive (*open circles*) and negative (*filled circles*) p_π basis function. The areas of the circles are proportional to the squares of the LCAO coefficients. The orbital notation is explained in the text

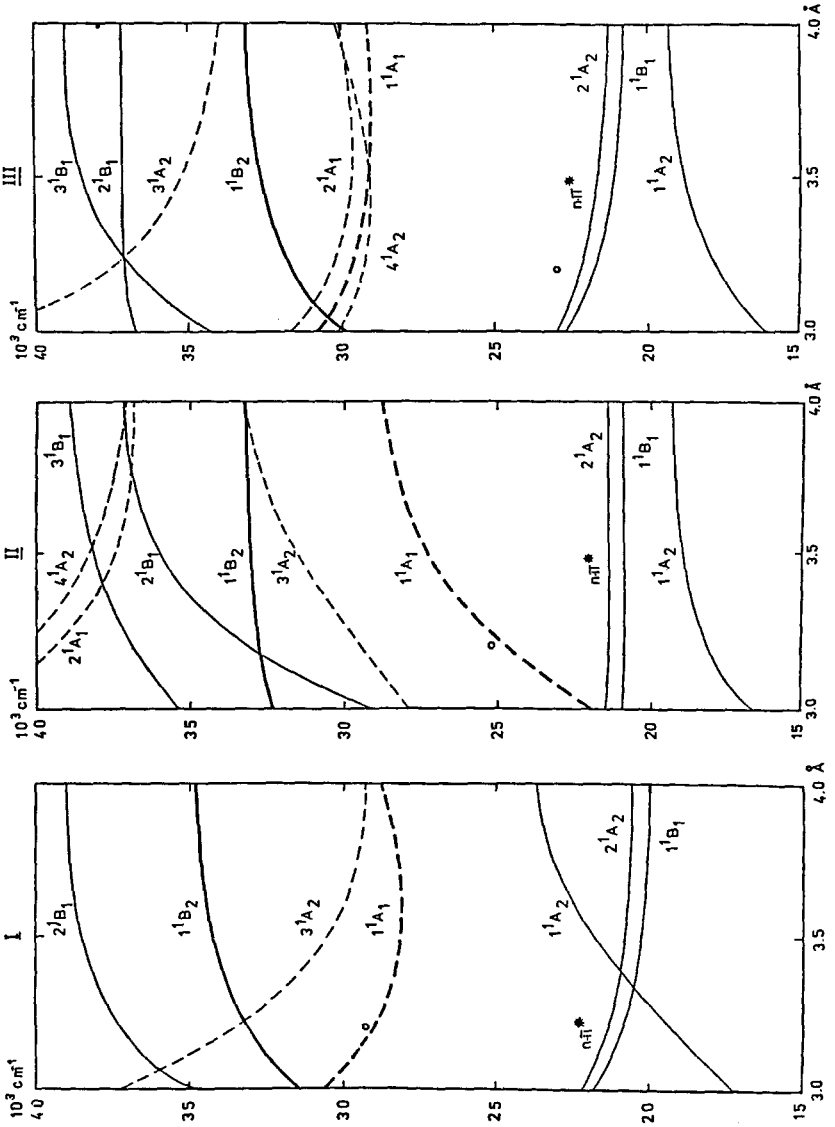

Fig. 4. The energy of transitions (cm^{-1}) as a function of inter-ring distance (Å) for models **I**, **II** and **III**. Except for two $n \to \pi^*$ transitions all transitions are the $\pi \to \pi^*$ type. *Dashed lines* denote the transitions of CT character ($\Delta q_Q \geq +0.5e$); *continuous lines* denote transitions localized on the rings, see Fig. 5. *Heavy lines* show the transitions of the oscillator strength $f \geq 0.001$; *thin lines* show the transitions of $f < 0.001$. The *circles* give the energy values of the longest wavelength absorption bands in **1**, **2** and **3**

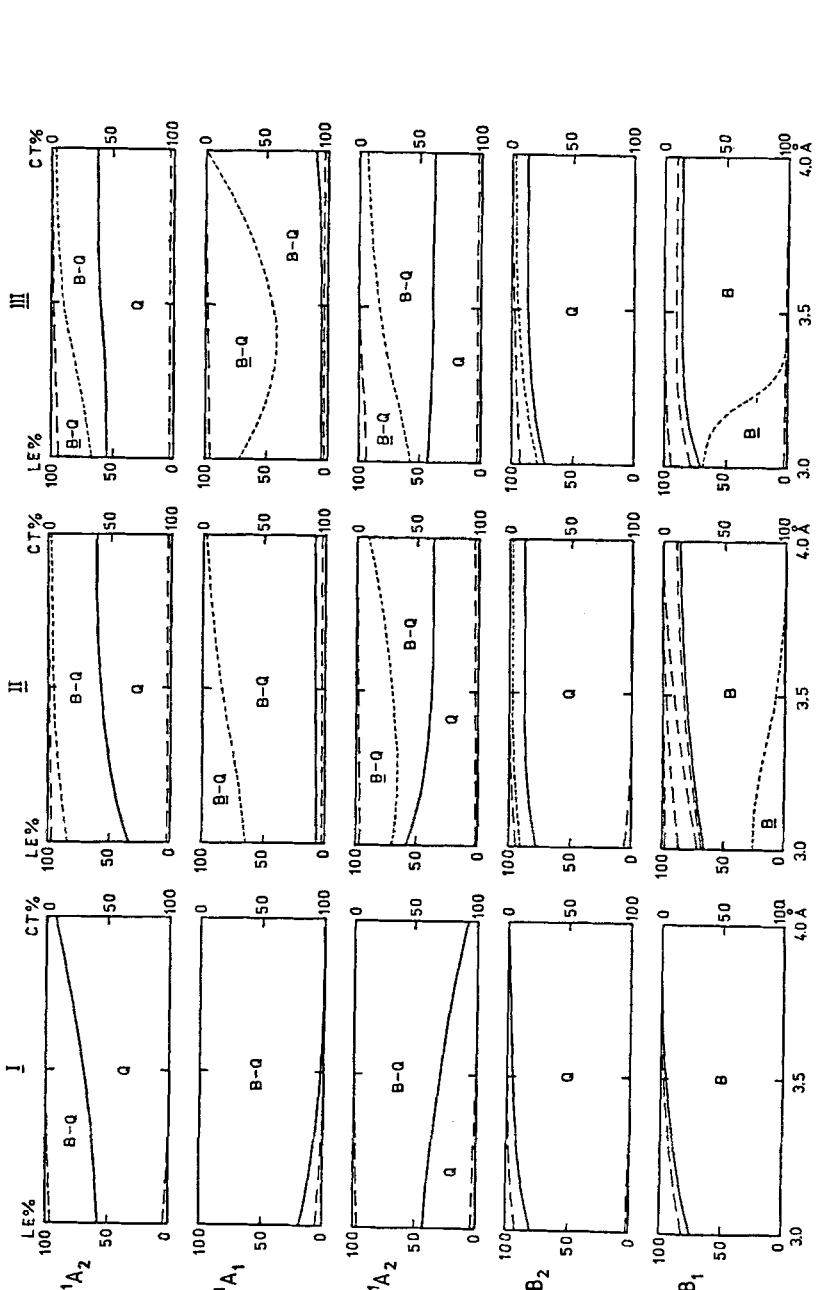

Fig. 5. Characteristics based on the transition density metrix method of the selected excited states in models **I**, **II** and **III** vs inter-ring distance. The symbols Q and B denote here the partial localization numbers l_Q and l_B. The symbols B–Q and B–Q denote the charge-transfer localization numbers $l_{B\to Q}$ and $l_{B\to Q}$, see the text. The weight of the locally excited states, LE%, is the sum of partial localization numbers. CT%, the sum of charge-transfer localization numbers, describes the weight of the CT states. LE% + CT% = 100%. *Continuous lines* separate the contribution of the LE and CT states in the excited state. *Dotted lines* separate the localization numbers of similar type (e.g. l_B and l_B or $l_{B\to Q}$ from $l_{B\to Q}$). *Dashed lines* separate the remaining localization numbers (e.g. l_Q from l_B and l_B, $l_{B\to Q}$ and $l_{B\to Q}$ from other)

Table 2. The size of the charge transfer Δq_Q (+e) into the Q ring versus inter-ring distance in the models **I**, **II** and **III** for the ground state and the selected excited states

States	Model I				Model II				Model III			
	3.0 Å	3.2 Å	3.5 Å	4.0 Å	3.0 Å	3.2 Å	3.5 Å	4.0 Å	3.0 Å	3.2 Å	3.5 Å	4.0 Å
Ground: $^1A_1$	0.11	0.06	0.02	0.00	0.08	0.07	0.06	0.06	0.13	0.11	0.08	0.06
Excited: 1^1A_2	0.36	0.35	0.27	0.07	0.61	0.50	0.40	0.36	0.34	0.35	0.35	0.35
Excited: 1^1A_1	0.81	0.91	0.97	0.99	0.91	0.92	0.92	0.91	0.91	0.94	0.96	0.91
Excited: 3^1A_2	0.51	0.59	0.70	0.93	0.37	0.51	0.61	0.60	0.51	0.53	0.58	0.59

greatest differences in the orbital energies appear only for the orbitals antisymmetrical with regard to the common symmetry plane (σ_{yz}). That plane goes through the oxygen atoms in the Q ring and carbon atoms located in the para positions of the B ring. The changes of orbital energy result from the appearance and then from an increase of the transannular interactions through-space, as a result of the increasing overlap of the π-electron clouds of the Q and B rings. As a consequence of that, the unambiguous localization of these orbitals on each of the rings is missing; e.g. the localization of $9b_1$ HOMO, for the distance of 3 Å, equals 55% on the B ring and 45% on the Q ring, almost as in the benzene dimer [10] or in PCP [9–11]. For the analogous $8b_1$ orbital the above ratios are reversed. This is the reason why the mentioned orbitals are denoted as a (B/Q) and a (Q/B), respectively; see Fig. 3 (right). As one would expect, the prevailing participation of the single excitations from the relevant orbitals in the wave function of the excited state would point to the appearance in this state of the transannular interactions.

Contrary to the antisymmetric orbitals, the symmetric orbitals show high degree of localization on one of the rings, independently of the inter-ring distance. For instance the $10b_2$ LUMO, denoted as s^*(Q) in Fig. 3, is localized on the Q ring. Total localization of the symmetric orbitals on one of the rings means that the total electron density accumulates on that ring. This is the reason why in these orbitals no electronic interactions appear between the Q and the B rings. Therefore, one might expect that the excited states in which the transfer of electron takes place from the B to the Q ring and the states in which the excitation is localized either on the Q or the B ring, will result from the electronic transitions between the symmetric orbitals.

According to the Mulliken theory [28], one of the reasons for the stabilization of the ground state in the CT complexes is the small charge transfer from $\boldsymbol{D}$ to $\boldsymbol{A}$. For all models such a stabilization really occurs. It is described by the value of the charge transferred in the ground state, see Table 2. The participation of the ionic ($\boldsymbol{D}^+\boldsymbol{A}^-$) structure increases along with the decrease of the inter-ring distance. It appears that model **III** is the most stable CT complex in the ground state. It is worth mentioning that HOMO in all models is not a pure HOMO of benzene which is required by the Mulliken theory. In addition, this represents an antisymmetric orbital, therefore is different from those in "intramolecular quinhydrones" [6], where HOMO is not only symmetrical but represents the pure HOMO of hyroquinone [18]. This difference has as its origin the transannular interactions and is responsible for the different scheme of electronic transitions in the B–Q complex as compared to the H–Q complex.

The results of calculations of the energy of transitions as a function of the inter-ring distances are given in Fig. 4. In all models each excited state is described by the symmetry of transition. The way in which all transitions were numbered originates from model **I** and was used for the remaining models. This facilitates the comparison of the results of calculations for the particular models although, as a result of this approach, the real sequence of transitions is not always preserved. For the reasons similar to those explained for a ground state, the analysis of the

low-lying excited states was carried out using the example of model **I**, with the discussion extended to models **II** and **III**.

Two $n \rightarrow \pi^*$ transitions take place into the 1^1B_1 and 2^1A_2 excited states. In model **I**, for the 4 Å distance, these are the lowest energy states. Their transition energies are similar and very much like those found in the single molecule of *p*-benzoquinone [18]. Along with decreasing of the inter-ring distance their energy slightly increases; however, for the distance below 3.3 Å they are no longer the states of lowest energy. This means that they behave in the same way as in the PCPQ **1**. The same happens both for models **II** and **III** (independently of the distance) and for the PCPQs **2** and **3**, see Table 1. The $n \rightarrow \pi^*$ transitions occur only inside of the Q ring, not being influenced by the inter-ring distance because they consist almost exclusively of single $n(Q) \rightarrow s^*(Q)$ excitations. As a result of this, they are totally localized on the Q ring, which also happens for models **II** and **III**.

The $\pi \rightarrow \pi^*$ transition to the 1^1A_1 excited state, to which particular attention is given in this paper, is marked by the reasonable large intensity and the decisive CT character, contrary to other transitions of the same type. The reason for it is, that the transition takes place only between the pair of symmetric orbitals $s(B)$ and $s^*(Q)$ (LUMO); therefore, according to Mulliken theory [28] the transition occurs between that pair of orbitals which fulfils the requirement of the greatest value of the overlap integrals for both orbitals involved. This is shown, in turn, by the fact that in each model, independently of the inter-ring distance, both the CT numbers $l_{B \rightarrow Q}$ (Fig. 5) and the size of the transferred charge Δq_Q (Table 2) take the largest values for the considered state. The behavior of this state will be considered for each model separately.

In model **I**, the intense CT transition slightly decreases first its energy along with the mutual approaching of the Q and the B rings. Then, after reaching a distance of 3.5 Å, the energy of the transition greatly increases. For 3.2 Å the transition energy (344.7 nm) is close to the experimental value in **1** (340 nm denoted on Fig. 4 by a dot) and $\Delta q_Q = +0.91e$. The inter-ring distance estimated on the base of the adjustment of energy of the CT transition is correct and is typical for this type of structure (phanes). The value of it was, therefore, assumed by us as a constant distance between the Q and B rings in models **II** and **III**. In model **II**, the energy of the discussed CT transition drastically decreases, which agrees with the observed substantial bathochromic shift of the long wavelength absorption band accompanying the transformation of **1** into **2**. For 3.2 Å, the transition occurs at 403.8 nm, as compared to the experimental value of 395 nm in **2**. The transfer of charge into the Q ring ($\Delta q_Q = +0.92e$) occurs mainly from the inner B ring ($\Delta q_B = -0.64e$) and from the outer B ring ($\Delta q_B = -0.28e$). Such a behavior of the CT transition results from the extension of the donor system and is similar to that expected for the real **2** structure. The CT transition in model **III** behaves quite differently from that in model **II**. It does not change its energy in the investigated range of the inter-ring distances, and assumes the energy close to the energy of CT transition in model **I**. Model **III** for the distance of 3.2 Å

represents the BQB system having a center of symmetry. The regarded transition takes place now at 336.9 nm, and the charge of $\Delta q_Q = +0.94e$ is equally transferred from both B rings (twice $\Delta q_B = -0.47e$). The calculated wavelength does not agree at all will the experimental value of the maximum of the long wavelength band absorption at 435 nm in **3**, which denies that the band has an exclusive CT character. As is shown in Fig. 4, the closest transitions with regard to the experimental maximum are two $n \rightarrow \pi^*$ transitions discussed earlier: 460.6 nm for the 1^1B_1 excited state and 452.1 nm for 2^1A_2 state. Moving to a real structure, i.e. from **III** to **3**, changes relative location of the CT transition and of $n \rightarrow \pi^*$ transitions. The latter are split as a result of the substituent effect. This supposition is made because the same split is characteristic for the $n \rightarrow \pi^*$ transitions of the tetramethyl derivative of *p*-benzoquinine as compared to *p*-benzoquinine [18]. However, the changes are small, in particular when compared to the $n \rightarrow \pi^*$ transition which has a non-zero intensity (1^1B state). The long wavelength absorption band in **3** was ascribed by us to that transition.

The transition to the 1^1A_2 excited state belongs to the same group as other $\pi \rightarrow \pi^*$ transitions. For model **I**, in the distance of 4 Å, i.e. for the separated Q and B molecules, this transition is located much above the $n \rightarrow \pi^*$ transitions and is localized on the Q ring. Considering its zero oscillator strength, the origin of this transition should be expected from the symmetry-forbidden long wavelength $\pi \rightarrow \pi^*$ transition in *p*-benzoquinone. Decrease of the inter-ring distance causes a remarkable decrease in the energy of the transition and its "shift" lifting it above the $n \rightarrow \pi^*$ transitions. This transition for distances below 3.3 Å becomes the one of the lowest energy and shows the decrease of the localization of excitation on the Q ring at the expense of the partial CT from the B to the Q ring. This tendency appears much stronger in model **II** and also exists in model **III**, see Fig. 5. The reason for such a behavior of the 1^1A_2 state is the increase of transannular interaction along with the mutual approach of the rings. In the wave function of the regarded state (considered for the example of model **I**), the essential contribution is due to that of the single excitation $a(B/Q) \rightarrow s^*(Q)$ and $a(Q/B) \rightarrow s^*(Q)$ in which the excitations from the HOMO prevail. This explains the origin of the longest wavelength state of 1^1A symmetry in PCPQs and also its differentiation, depending on the type of complex.
Similar discussion may be presented for the 3^1A_2 excited state because of the identical symmetry of both states. However, as can be seen in Fig. 5, the ratio of the localization numbers l_Q and $l_{B \rightarrow Q}$ is now reversed. Therefore, this state shows a predominating CT character, see also Table 2. Along with the decrease of inter-ring distance, this character changes in favor of the local excitation of the Q ring. Also here, this is caused by the transannular interactions.

The second $\pi \rightarrow \pi^*$ transition of significant intensity, greater than that of the CT transition, represents a transition to the 1^1B_2 excited state (mainly the single excitation $s(Q) \rightarrow s^*(Q)$). The latter is almost entirely localized on the Q ring and is independent of the model under consideration. This suggests that the transition originates from the symmetry-allowed, intense, short wavelength transition in *p*-benzoquinone, with regard to which it is shifted bathochromically. The greatest

shift occurs for model **III**. The corresponding absorption band is observed in the UV-VIS spectra of all PCPQs in the 250–300 nm region. In fact, for **3** this band shows the greatest shift to the red.

Finally let us pay attention to the transition to the 2^1B_1 excited state. This transition is localized on the B ring(s), see Fig. 5. It originates from the transition corresponding to the α band in benzene and it is bathochromically shifted with regard to the latter. The energy of the transition to the 2^1B_1 state is in all models greater than the energy of the transition to the 1^1B_2 state. The fact that the real structure is considered, is responsible for a decrease of the energy of the 2^1B_1 transition in all PCPQs. The 2^1B_1 state moves ahead of the 1^1B_2 state, localized on the Q ring. This change arises from transannular interactions and beside that from the substituent effect, which is reflected in the shoulder of the absorption curves in the region ca. 300 nm.

5. Conclusions

The application of the all-valence-electron approach (in form of the CNDO/S method), together with the analysis of the excited states by the transition density matrix method, allowed us to determine the character of the band of the long wavelength absorption in the double-layered and triple-layered [2.2]paracylophanequinones. The presence in these compounds of benzene ring(s) as donor and *p*-benzoquinone ring as acceptor implies a necessity to consider these structures as the intramolecular charge-transfer complexes. It also makes necessary the application of the stacked, planar rings not connected by ethane bridges as the model structures for calculations. The close relation of these models to the investigated PCPQs helps one to conclude that in **1** and **2** the regarded longest wavelength absorption band originates from the intramolecular charge transfer, while in **3** it mainly originates from the $n \rightarrow \pi^*$ transitions in *p*-benzoquinone ring.

The intramolecular ***DAD*** complex based on model **III** shows its highest stability in the ground state and the greatest electron transfer in the CT excited state. These are the properties desired for molecular information carriers [12].

References

1. Cram DJ, Day AC (1966) J Org Chem 31:1227
2. Rebafka W, Staab HA (1973) Angew Chem 85:831; Rebafka W, Staab HA (1974) Angew Chem 86:234; Rebufka W, Staab HA (1973) Angew Chem Int Ed Engl 12:776; Rabafka W, Staab HA (1974) Angew Chem Int Ed Engl 13:203; Staab HA, Herz CP, Henke H-E (1974) Tetrahedron Lett 4393; Staab HA, Haffner H (1974) Tetrahedron Lett 4397
3. Tatemitsu H, Otsubo T, Sakata Y, Misumi S (1975) Tetrahedron Lett 3059
4. Misumi S, Otsubo T (1978) Acc Chem Res 11:251
5. Vogler H, Ege G, Staab HA (1975) Tetrahedron 31:2441; Vogler H, Ege G, Staab HA (1977) Mol Phys 33:923

6. Vogler H (1983) Z Naturforsch 38B:1130
7. Vogler H (1983) Croat Chim Acta 56:297
8. (a) McWeeny R, Sutcliffe BT (1969) Methods of molecular quantum mechanics. Academic Press, London New York
(b) Mestechkin MM (1977) The density matrix method in molecular theory (in Russian). Naukova Dumka, Kiev
9. Wisor AK, Czuchajowski L (1986) J Phys Chem 90:1541; Wisor AK, Czuchajowski L (1986) J Phys Chem 90:3964
10. Czuchajowski L, Wisor AK (1988) Theochem 165:163
11. Czuchajowski L, Wisor AK (1987) J Electron Spectrosc Relat Phenom 43:169
12. Stolarczyk LZ, Piela L (1984) Chem Phys 85:451
13. Koutecky J, Paldus J (1962) Collect Czech Chem Commun 27:599; Koutecky J, Paldus J (1963) Theor Chim Acta 1:268
14. Czuchajowski L, Pietrzycki W (1978) J Mol Struct 47:423; Czuchajowski L, Wisor AK, Maslankiewicz MJ (1981) Monatsh Chem 112:1175; Wisor AK, Czuchajowski L (1983) Monatsh Chem 114:1023; Wisor AK, Kus P, Czuchajowski L (1983) Monatsh Chem 114:1213
15. Gleiter R (1969) Tetrahedron Lett 4453
16. Del Bene J, Jaffe HH (1968) J Chem Phys 48:1807; Del Bene J, Jaffe HH (1968) J Chem Phys 48:4050; Del Bene J, Jaffe HH (1968) J Chem Phys 49:1221; Del Bene J, Jaffe HH (1969) J Chem Phys 50:563; Del Bene J, Jaffe HH (1969) J Chem Phys 50:1126; Ellis RL, Kuehnlenz G, Jaffe HH (1972) Theor Chim Acta 26:131; Kuehnlenz G, Jaffe HH (1973) J Chem Phys 58:2238
17. Vogler H (1981) Theor Chim Acta 60:65
18. Wisor AK, unpublished results
19. Trommsdorff HP (1972) J Chem Phys 56:5358; Merienne-Lafore MF, Trommsdorff HP (1976) J Chem Phys 64:3791; Bigelow RW (1978) J Chem Phys 68:5068
20. Jacques P, Faure J, Chalvet O, Jaffe HH (1981) J Phys Chem 85:473
21. (a) Beppu Y, Ninomiya I (1982) Comput Chem 6:87
(b) Wisor AK (1986) Comput Chem 10:307
22. (a) Luzaanov AV, Sukhorukov AA, Umanskii VE (1974) Teor Eksp Khim 10:456
(b) Luzanov AV (1977) Teor Eksp Khim 13:579
(c) Luzanov AV, Pedash VF (1979) Teor Eksp Khim 15:436
(d) Luzanov AV (1980) Usp Khim 49:2086
23. (a) Longuet-Higgins HC, Murrell JN (1955) Proc Phys Soc A68:901; Longuett-Higgins HC, Murrell JN (1955) Proc Phys Soc A68:969; Godefrey M, Murrell JN (1964) Proc Roy Soc A278:64
(b) Baba, H, Suzuki S, Takemura T (1969) J Chem Phys 50:2078
(c) Edmiston C, Ruedenberg K (1963) Rev Mod Phys 34:457; Edmiston C, Ruedenberg K (1965) J Chem Phys 43:597; England W, Salmon LS, Ruedenberg K (1971) Top Curr Chem 23:31
(d) Ohta T, Kuroda H, Kunii T (1970) Theor Chim Acta 19:167
(e) Sukhorukov AA, Umanskii VE, Sadorozhnii BA, Lavrushin VF (1976) Teor Eksp Khim 12:681
(f) Fratev F, Polansky OE, Mehlhorn A, Monev V (1979) J Mol Struct 56:245; Fabian J, Mehlhorn A, Fratev F (1980) Int J Quantum Chem 17:235
24. Brown CJ (1953) J Chem Soc 3265; Lonsdale K, Milledge JJ, Rao KVK (1960) Proc Roy Soc A255:82; Hope H, Bernstein J, Trueblood KN (1972) Acta Crystallogr B28:1733
25. Irngartinger H, Acker R-D, Rebafka W, Staab HA (1974) Angew Chem 86:705; Irngartinger H, Acker R-D, Rebafka W, Staab HA (1974) Angew Chem Int Ed Engl 13:674
26. Trotter J (1960) Acta Crystallogr 13:26; Hagen K, Hedberg K (1973) J Chem Phys 59:156
27. Mizuno H, Nishiguchi K, Otsubo T, Misumi S, Morimoto N (1972) Tetrahedron Lett 4981; Otsubo T, Mizogami S, Otsubo I, Tozuka Z, Sakagami A, Sakata Y, Misumi S (1973) Bull Chem Soc Jpn 46:3519; Mizuno H, Nishiguchi K, Toyoda T, Otsubo T, Misumi S, Morimoto N (1977) Acta Crystallogr B33:329
28. (a) Mulliken RS, Person WB (1969) Molecular complexes, A Lecture and Reprint Volume. Wiley, New York
(b) Briegleb G (1961) Elektronen-Donator-Acceptor Komplexe. Springer, Berlin Göttingen Heidelberg